Journal of Power Electronics (2023) 23:1517–1528
https://doi.org/10.1007/s43236-023-00649-5

ORIGINAL ARTICLE

Dynamic power distribution strategy using multi-objective collaborative optimization for hybrid energy storage systems

Yuqing Shao[1] · Hongjuan Zhang[1] · Yan Gao[1] · Baoquan Jin[2]

Received: 30 December 2022 / Revised: 7 May 2023 / Accepted: 9 May 2023 / Published online: 31 May 2023

Abstract

This paper proposes a dynamic power distribution strategy for the hybrid energy storage systems (HESSs) in electric vehicles (EVs). First, the power loss of a HESS is analyzed based on its structure and model. Second, the optimal objectives for EV range extension, battery degradation mitigation, and HESS energy loss reduction are set, and the corresponding optimization variables are determined. Then, a multi-objective collaborative optimization (MOCO) function is established. It is further transformed into a linear programming problem with the battery current as the control variable. Finally, the dynamic power distribution scheme is obtained by analyzing the MOCO problem. The dynamic power distribution strategy using the MOCO is studies through simulations and experiments under the worldwide harmonized light vehicles test cycle. The obtained results indicate that the performances of the three optimal objectives are collaboratively improved.

Keywords Hybrid energy storage system · Multi-objective collaborative optimization · Electric vehicle · Power distribution

1 Introduction

To achieve carbon neutrality, emissions reductions in the power and transportation sectors need to be accelerated [1]. As a promising option in low-carbon transportation, electric vehicles (EVs) use batteries to form an energy storage system (ESS). Nevertheless, batteries have defects such as low specific power, short cycle life, and narrow operating temperature range [2]. EVs require high power charging and discharging under extreme operating conditions such as rapid acceleration and emergency braking. In the process, batteries can fall short or be severely damaged. In addition, the safety of the batteries in EVs has been questioned given the frequent occurrence of extreme weather around the world. Therefore, the development of ESSs is crucial for EVs. It is well known that supercapacitors (SCs) have the advantages of high power density, long cycle life, and wide operating temperature range [3]. The properties of SCs can compensate for many of the defects found in batteries. Therefore, battery/SC hybrid energy storage systems (HESSs) have been widely studied in recent years.

In HESS literature, power distribution strategy design is a key issue that has received the most attention [4]. A properly designed power distribution strategy can fully exploit the advantages of HESSs, which extends the EV range and protects the battery [5]. Moreover, it can reduce the energy loss to achieve the goal of low carbon emissions. Thus, a great deal of research has been done on power distribution strategies. There are two classical power distribution strategies: the split-frequency method and the power-level method [6]. In the split-frequency method, the demand power is segmented into two parts. The low-frequency part, which is borne by the battery; and the high-frequency part, which is borne by the SC [7]. For example, Peng et al. [8] achieved battery protection using this approach. In the power-level method, power is distributed according to the demand power [9]. For instance, Li et al. [10] reduced system energy loss in this way. However, these strategies follow pre-set rules and cannot guarantee the optimal power distribution scheme at any moment. Therefore, power distribution strategies with optimal objectives have been proposed and studied. These strategies are more flexible and targeted, which means they can better cope with the complex working conditions of EVs. Optimal objectives are proposed according to the

✉ Hongjuan Zhang
zhanghongjuan@tyut.edu.cn

[1] College of Electrical and Power Engineering, Taiyuan University of Technology, Shanxi, China

[2] Key Laboratory of Advanced Transducers and Intelligent Control System, Ministry of Education, Taiyuan University of Technology, Shanxi, China

system parameters, and performance optimization is realized according to certain constraints [11]. EV range extension, battery degradation mitigation, and HESS energy loss reduction are the three mainstream optimal objectives in power distribution strategies. Their research is reviewed and analyzed below.

EV range extension is the biggest concern for most consumers. Naseri et al. [12] recovered EV braking energy through the SC in a HESS and reused it. Braking energy was wasted when battery energy storage system (BESS) worked alone. However, a BESS can also recover braking energy with the development of ESS. In addition, with the HESS, the EV range is naturally extended with an increase of the ESS capacity. Therefore, many researchers have stated that the range of an EV can be effectively extended using a HESS [13, 14]. They do not consider the impact of different battery and SC characteristics on EV range extension. They also do not consider the impact of different power distribution strategies on EV range extension. Studies of these kinds have not been presented in the literature. The superiority of HESS in terms of EV range extension is verified more objectively in this paper.

When an EV is moving, high current and frequent current variations drastically shorten battery life and can result in safety problems [15]. Therefore, battery protection extends battery life and indirectly ensures driving safety. To quantify battery protection, battery degradation is generally used in studies. Li et al. [16] used Ah-throughput to estimate battery degradation and to minimized the Ah-throughput in offline size optimization. This is effective in protecting the battery from current spikes. Song et al. [17] incorporated Ah-throughput into the cost function, which achieved a battery degradation reduction. Root mean square (RMS) is often used to represent the change rate [18]. In [19], battery degradation was mitigated by reducing the RMS of battery current. Wang et al. [20] chose the RMS of current to indicate battery degradation. The result was minimized for battery life extension. The studies cited above considered the magnitude or change rate alone. However, this cannot comprehensively indicate battery degradation. Furthermore, battery degradation should be involved as an online factor during power distribution. In a nutshell, battery protection can be achieved by the two points. In this paper, the effects of the current magnitude and change rate on battery degradation are considered together. Then, battery degradation is considered in the online optimization process.

In addition to range extension and battery protection, reducing energy loss is also an important objective. In general, energy loss can be assessed by real-time power loss [21]. HESS loss is composed of the losses of the batteries, SCs, and direct current to direct current (DC/DC) converters. Cheng et al. [22] considered the battery and SC losses. Li et al. [23] considered the battery, SC, and DC/DC converter losses, but used an empirical curve to calculate the loss of the DC/DC converter. Similarly, Wang et al. [24] assumed a constant efficiency of the DC/DC converter for loss calculation. Shen et al. [25] used a DC/DC converter model that included switching loss when calculating losses. In power distribution strategies, considering real-time power loss is beneficial to the objective of energy loss reduction.

By optimizing one of the three objectives, the above literature has improved the performance of EVs to a certain extent. However, there are contradictions in HESSs when the three objectives are expected to be achieved simultaneously. The one-sided optimization of one can lead to the deterioration of the others. Specifically, Anbazhagan et al. [26] proposed that the addition and use of SCs can extend EV range, mitigate battery degradation, and reduce battery loss. However, more losses were incurred due to the addition of an SC ESS. Therefore, it is difficult to make all of the objectives optimal at the same time. A compromise among conflicting objectives is inevitable. It is necessary to design an optimization method. The required method needs to be more universal and flexible than rule-based methods. It also needs to be faster and more efficient than intelligent algorithms. In this paper, a dynamic power distribution strategy is proposed as a solution to address this problem. In the proposed dynamic power distribution strategy, multi-objective collaborative optimization (MOCO) is used to find an optimal solution in real time. In the power distribution scheme using this solution, the three optimal objectives are kept at the collaborative optimum at all times. Thus, on the basis of battery safety and EV range extension, the system efficiency is improved. The dynamic power distribution between the batteries and the SCs is finally completed.

The remainder of this paper is organized as follows. In Sect. 2, the HESS is modeled and its power loss is analyzed. Section 3 details a dynamic power distribution strategy using the MOCO. Section 4 and Sect. 5 verify the proposed strategy through simulation and experimental results, respectively. Finally, the conclusion is presented in Sect. 6.

2 System description

2.1 HESS structure and model

The HESS adopts the active parallel structure illustrated in Fig. 1a. The battery serves as the main power, while the SC serves as the auxiliary power. They are connected to the direct current (DC) bus via two DC/DC converters. The battery and DC/DC converter 1 constitute the BESS. The SC and DC/DC converter 2 constitute the SC ESS. As shown in Fig. 1b, the battery, SC, and DC/DC converter are described by equivalent circuit models. Hence, the equations of the HESS can be deduced as:

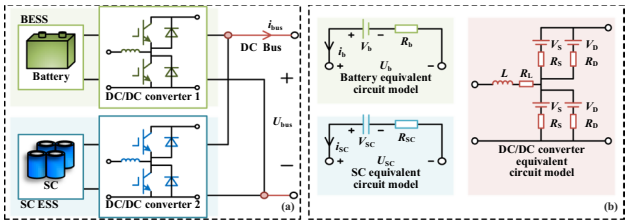

Fig. 1 Diagrams showing: **a** HESS structure; **b** equivalent circuit models

$$\begin{cases} U_{\mathrm{b}} = V_{\mathrm{b}} - R_{\mathrm{b}} i_{\mathrm{b}} \\ U_{\mathrm{SC}} = V_{\mathrm{SC}} - R_{\mathrm{SC}} i_{\mathrm{SC}} \\ P_{\mathrm{bus}} = U_{\mathrm{bus}} i_{\mathrm{bus}} \\ i_{\mathrm{bus}} = i_{\mathrm{b}} + i_{\mathrm{SC}} \\ SOC_{\mathrm{b}} = SOC_{\mathrm{b0}} - \int i_{\mathrm{b}} \mathrm{d}t / 3600Q \\ SOC_{\mathrm{SC}} = SOC_{\mathrm{SC0}} - \int i_{\mathrm{SC}} \mathrm{d}t / CU_{\mathrm{SCN}} \end{cases} \tag{1}$$

where U_{b} is the battery terminal voltage. V_{b} is the battery open-circuit voltage. R_{b} is the battery internal resistance. i_{b} is the battery current. SOC_{b} is the state of charge (SOC) of the battery. Q is the battery rated capacity. U_{SC}, V_{SC}, R_{SC}, i_{SC}, and SOC_{SC} are the same variables for the SC. P_{bus}, U_{bus}, and i_{bus} are the power, voltage, and current in the DC bus. SOC_{b0} and SOC_{SC0} are the initial SOC of the battery and SC, respectively. C is the SC rated capacitance. U_{SCN} is the SC rated voltage.

2.2 HESS power loss analysis

According to the models, the power losses of the BESS and SC ESS are presented in Eqs. (2) and (3). $P_{\mathrm{BESS\_loss}}$ and $P_{\mathrm{SC\_ESS\_loss}}$ indicate the power losses of the BESS and SC ESS, respectively.

$$\begin{aligned} P_{\mathrm{BESS\_loss}} &= R_{\mathrm{b}} i_{\mathrm{b}}^2 + R_{\mathrm{L}} i_{\mathrm{b}}^2 + D_1 \left(R_{\mathrm{S}} i_{\mathrm{b}}^2 + V_{\mathrm{S}} |i_{\mathrm{b}}| \right) \\ &\quad + \left(1 - D_1\right) \left(R_{\mathrm{D}} i_{\mathrm{b}}^2 + V_{\mathrm{D}} |i_{\mathrm{b}}| \right) + f_{\mathrm{s}} \left(P_{\mathrm{on}} + P_{\mathrm{off}} \right) \end{aligned} \tag{2}$$

$$\begin{aligned} P_{\mathrm{SC\_ESS\_loss}} &= R_{\mathrm{SC}} i_{\mathrm{SC}}^2 + R_{\mathrm{L}} i_{\mathrm{SC}}^2 + D_2 \left(R_{\mathrm{S}} i_{\mathrm{SC}}^2 + V_{\mathrm{S}} |i_{\mathrm{SC}}| \right) \\ &\quad + \left(1 - D_2\right) \left(R_{\mathrm{D}} i_{\mathrm{SC}}^2 + V_{\mathrm{D}} |i_{\mathrm{SC}}| \right) + f_s \left(P_{\mathrm{on}} + P_{\mathrm{off}} \right) \end{aligned} \tag{3}$$

where D_1 and D_2 are the duty ratios of the IGBTs in DC/DC converter 1 and DC/DC converter 2, and $D_1 = U_{\mathrm{b}} / U_{\mathrm{bus}}$ and $D_2 = U_{\mathrm{SC}} / U_{\mathrm{bus}}$. R_{S}, R_{L}, and R_{D} are the equivalent resistances of the IGBTs, inductors, and diodes, respectively. V_{S} and V_{D} are the turn-on voltages of the IGBTs and diodes, respectively. f_{s} is the switching frequency of the DC/DC converters. P_{on} and P_{off} are the turn-on loss and turn-off loss of the IGBTs.

In this paper, p and q indicate the operating states of the BESS and the SC ESS, respectively. They are defined as:

$$p, q = \begin{cases} 1, \text{ discharge state} \\ -1, \text{ charge state} \end{cases} \tag{4}$$

The HESS power loss can be derived as:

$$\begin{aligned} P_{\mathrm{loss}} &= P_{\mathrm{BESS\_loss}} + P_{\mathrm{SC\_ESS\_loss}} \\ &= \left[R_{\mathrm{b}} + R_{\mathrm{L}} + \frac{U_{\mathrm{b}}}{U_{\mathrm{bus}}} R_{\mathrm{S}} + \left(1 - \frac{U_{\mathrm{b}}}{U_{\mathrm{bus}}}\right) R_{\mathrm{D}} \right] i_{\mathrm{b}}^2 \\ &\quad + p \left[\frac{U_{\mathrm{b}}}{U_{\mathrm{bus}}} V_{\mathrm{S}} + \left(1 - \frac{U_{\mathrm{b}}}{U_{\mathrm{bus}}}\right) V_{\mathrm{D}} \right] i_{\mathrm{b}} + f_{\mathrm{s}} \left(P_{\mathrm{on}} + P_{\mathrm{off}} \right) \\ &\quad + \left[R_{\mathrm{SC}} + R_{\mathrm{L}} + \frac{U_{\mathrm{SC}}}{U_{\mathrm{bus}}} R_{\mathrm{S}} + \left(1 - \frac{U_{\mathrm{SC}}}{U_{\mathrm{bus}}}\right) R_{\mathrm{D}} \right] i_{\mathrm{SC}}^2 \\ &\quad + q \left[\frac{U_{\mathrm{SC}}}{U_{\mathrm{bus}}} V_{\mathrm{S}} + \left(1 - \frac{U_{\mathrm{SC}}}{U_{\mathrm{bus}}}\right) V_{\mathrm{D}} \right] i_{\mathrm{SC}} + f_{\mathrm{s}} \left(P_{\mathrm{on}} + P_{\mathrm{off}} \right) \\ &= A i_{\mathrm{b}}^2 + B i_{\mathrm{b}} + C \end{aligned} \tag{5}$$

where

$$\begin{aligned} A &= R_{\mathrm{b}} + R_{\mathrm{SC}} + 2R_{\mathrm{L}} + \frac{U_{\mathrm{b}} + U_{\mathrm{SC}}}{U_{\mathrm{bus}}} R_{\mathrm{S}} + \left(2 - \frac{U_{\mathrm{b}} + U_{\mathrm{SC}}}{U_{\mathrm{bus}}}\right) R_{\mathrm{D}} \\ B &= (p - q) V_{\mathrm{D}} + \left(p U_{\mathrm{b}} - q U_{\mathrm{SC}} \right) \frac{V_{\mathrm{S}} - V_{\mathrm{D}}}{U_{\mathrm{bus}}} \\ &\quad - 2 \left[R_{\mathrm{SC}} + R_{\mathrm{L}} + \frac{U_{\mathrm{SC}}}{U_{\mathrm{bus}}} R_{\mathrm{S}} + \left(1 - \frac{U_{\mathrm{SC}}}{U_{\mathrm{bus}}}\right) R_{\mathrm{D}} \right] i_{\mathrm{bus}} \\ C &= \left[R_{\mathrm{SC}} + R_{\mathrm{L}} + \frac{U_{\mathrm{SC}}}{U_{\mathrm{bus}}} R_{\mathrm{S}} + \left(1 - \frac{U_{\mathrm{SC}}}{U_{\mathrm{bus}}}\right) R_{\mathrm{D}} \right] i_{\mathrm{bus}}^2 \\ &\quad + q \left[\frac{U_{\mathrm{SC}}}{U_{\mathrm{bus}}} V_{\mathrm{S}} + \left(1 - \frac{U_{\mathrm{SC}}}{U_{\mathrm{bus}}}\right) V_{\mathrm{D}} \right] i_{\mathrm{bus}} + 2 f_{\mathrm{s}} \left(P_{\mathrm{on}} + P_{\mathrm{off}} \right) \end{aligned}$$

2.3 EV model

Assuming an EV is driving on a flat road, its dynamic model is constructed as follows:

$$m_{\mathrm{EV}} g f v + \frac{1}{2} C_{\mathrm{D}} A_{\mathrm{EV}} \rho v^3 + m_{\mathrm{EV}} v \frac{\mathrm{d}v}{\mathrm{d}t} = P_{\mathrm{bus}} \left(\eta_{\mathrm{T}} \eta_{\mathrm{m}} \right)^{\mathrm{i}} \tag{6}$$

where the EV parameters are defined in Table 1. v is the speed of the EV. i is the operating state of the EV, which is defined as:

$$i = \begin{cases} 1, \text{driving state} \\ 0, \text{stop state} \\ -1, \text{braking state} \end{cases} \tag{7}$$

Table 1 EV parameters

Parameters	Symbol	Value	Unit
EV mass	m_{EV}	1600	kg
Gravitational acceleration	g	9.8	m/s^2
Rolling resistance coefficient	f	0.01	
Air drag coefficient	C_D	0.24	
Front area	A_{EV}	2.67	m^2
Air density	ρ	1.2	kg/m^3
Motor efficiency	η_m	95	%
Transmission efficiency	η_T	95	%

To evaluate the performance of EVs, a test cycle standard needs to be used. The most classic test cycle standard, the New European Driving Cycle, is too idealized and too far from actual situations. Meanwhile, the Worldwide harmonized Light vehicles Test Cycle (WLTC) is more in line with the realities of EVs. The driving conditions are diverse and complex in the WLTC. It incorporates the acceleration, deceleration, stopping, and braking of an EV. The transition between these conditions is frequent and rapid.

In this paper, the WLTC is selected as the test cycle. The WLTC simulates a 23.3 km route in 30 min. The test cycle is divided into four stages: a low-speed part, a medium-speed part, a high-speed part, and an extra high-speed part. The four stages correspond to urban condition, suburban condition, rural condition, and highway condition for EVs. The durations are 589 s, 433 s, 455 s, and 323 s, respectively.

The EV model converts the given speed into the demand power [27]. The given vehicle speed and calculated demand power are shown in Fig. 2. A positive power means that the HESS outputs power to drive the EV, while a negative power means that the EV feeds energy back to the HESS. By integrating the two parts during the test cycle, it can be seen that the driving energy in the DC bus is 13089 kJ, and that the braking energy in the DC bus is 2849 kJ.

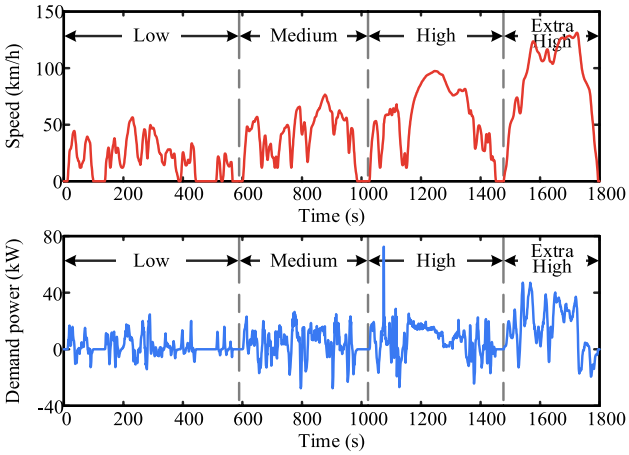

Fig. 2 Given vehicle speed and calculated demand power

3 Dynamic power distribution strategy

A dynamic power distribution strategy using the MOCO is proposed to achieve scheduling of the BESS and SC ESS in the HESS. The framework is shown in Fig. 3. The strategy is described in detail below.

3.1 Multi-objective optimization problem

Three optimal objectives are considered in this strategy: EV range extension, battery degradation mitigation, and HESS energy loss reduction. The optimal objectives are analyzed separately to identify the optimization variables.

1. Optimal Objectives 1: EV Range Extension

EV range depends on the capacity of the battery. The consumption of battery capacity can be measured by the battery SOC drop. The less the SOC drops, the longer the EV range. According to (1), the SOC drop of the battery can be written as:

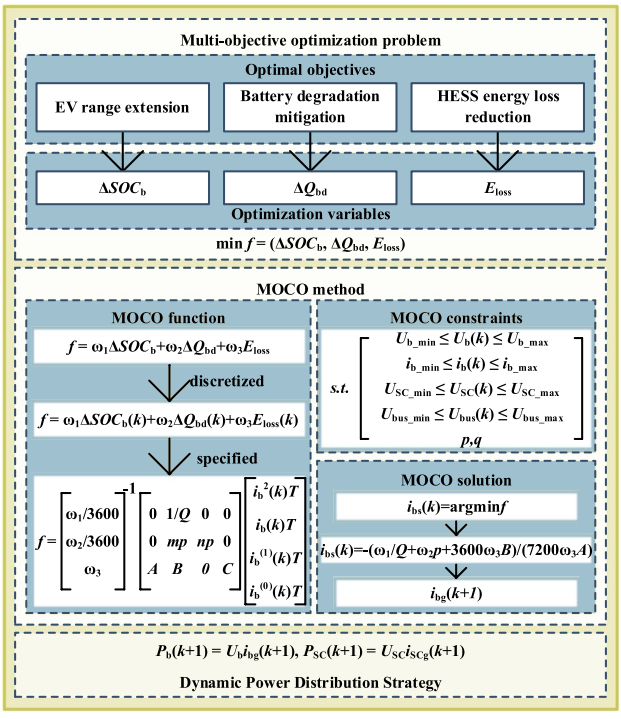

Fig. 3 Framework of the dynamic power distribution strategy using MOCO

$$\Delta SOC_{\mathrm{b}} = \frac{1}{3600Q}\int i_{\mathrm{b}}\mathrm{d}t \tag{8}$$

Accordingly, by reducing the battery SOC drop, the objective of extending EV range is naturally achieved.

2. Optimal Objective 2: Battery Degradation Mitigation

In battery degradation calculation, two factors are taken into account. One factor is the Ah-throughput of the battery current. The other is the change rate throughput of the battery current. When merging the two factors by additive weighting, the formula to quantify battery degradation is defined as:

$$\Delta Q_{\mathrm{bd}} = m\Delta Q_{\mathrm{b}} + n\Delta Q'_{\mathrm{b}} \tag{9}$$

where

$$\Delta Q_{\mathrm{b}} = \frac{1}{3600}\int |i_{\mathrm{b}}|\mathrm{d}t$$
$$\Delta Q'_{\mathrm{b}} = \frac{1}{3600}\int |i'_{\mathrm{b}}|\mathrm{d}t$$

ΔQ_{b} is the Ah-throughput of the battery current. ΔQ_{b}' is the change rate throughput of the battery current. m and n denote the weight factors of ΔQ_{b} and ΔQ_{b}' in ΔQ_{bd}, and $m+n=1$ is specified.

In brief, the objective of mitigating battery degradation can be achieved by reducing ΔQ_{bd}. The specific approach is to reduce the magnitude and change rate of the battery current.

3. Optimal Objective 3: HESS Energy Loss Reduction

The energy loss of the HESS varies dynamically when its mode switches. By integrating the real-time power loss, the HESS energy loss can be calculated as:

$$E_{\mathrm{loss}} = \int P_{\mathrm{loss}}\mathrm{d}t \tag{10}$$

According to Eq. (5), the HESS energy loss is a dynamic function of the battery current. Consequently, the objective of reducing the HESS energy loss can be achieved by controlling the battery current.

4. Multi-Objective Optimization Problem

Based on the above analysis, ΔSOC_{b}, ΔQ_{bd} and E_{loss} are selected as optimization variables. Finally, a multi-objective optimization problem with three variables is obtained, which can be expressed as:

$$\min f(\Delta SOC_{\mathrm{b}}, \Delta Q_{\mathrm{bd}}, E_{\mathrm{loss}}) \tag{11}$$

3.2 MOCO method

To solve the multi-objective optimization problem, MOCO is adopted. First, a MOCO function is constructed. Then, constraints are specified for the function. Finally, the MOCO solution is obtained by solving the constrained function.

1. MOCO Function

By additive weighting, the multi-objective optimization problem is transformed into a MOCO function:

$$f = \omega_1\Delta SOC_{\mathrm{b}} + \omega_2\Delta Q_{\mathrm{bd}} + \omega_3 E_{\mathrm{loss}} \tag{12}$$

where the weight factors ω_1, ω_2, and ω_3 are set to normalize the optimization variables on different scales. Their values are determined by the sizes of the three parts.

To solve the function, a multi-step decision is used. It has to reach the minimum at each step. At each sampling time, the solution for the next step is determined. At the kth sampling time, the MOCO function is discretized as:

$$\begin{aligned} f &= \omega_1\Delta SOC_{\mathrm{b}}(k) + \omega_2\Delta Q_{\mathrm{bd}}(k) + \omega_3 E_{\mathrm{loss}}(k) \\ &= \begin{bmatrix} \omega_1/3600 \\ \omega_2/3600 \\ \omega_3 \end{bmatrix}^{-1} \begin{bmatrix} 0 & 1/Q & 0 & 0 \\ 0 & mp & np & 0 \\ A & B & 0 & C \end{bmatrix} \begin{bmatrix} i_{\mathrm{b}}^2(k)T \\ i_{\mathrm{b}}(k)T \\ i_{\mathrm{b}}^{(1)}(k)T \\ i_{\mathrm{b}}^{0}(k)T \end{bmatrix} \end{aligned} \tag{13}$$

where T is the sampling time.

2. MOCO Constraints

$$s.t. \begin{cases} U_{\mathrm{b\_min}} \le U_{\mathrm{b}}(k) \le U_{\mathrm{b\_max}} \\ i_{\mathrm{b\_min}} \le i_{\mathrm{b}}(k) \le i_{\mathrm{b\_max}} \\ U_{\mathrm{SC\_min}} \le U_{\mathrm{SC}}(k) \le U_{\mathrm{SC\_max}} \\ U_{\mathrm{bus\_min}} \le U_{\mathrm{bus}}(k) \le U_{\mathrm{bus\_max}} \\ p, q \end{cases} \tag{14}$$

The constraints for the parameters in (13) are listed in (14).

3. MOCO Solution

As can be seen in Eq. (13), the MOCO function is a nonlinear function with the battery current as a variable. Real-time measurement values are used to calculate it. Therefore, variables other than the battery current are treated as constants. At the kth sampling time, the MOCO solution $i_{\mathrm{bs}}(k)$ is given as follows:

$$i_{bs}(k) = \arg\min f \tag{15}$$

The MOCO function is essentially a quadratic function of the battery current. Thus, Eq. (15) can also be written as follows:

$$f'\left[i_{bs}(k)\right] = 0 \tag{16}$$

According to Eqs. (13) and (16), the expression of the MOCO solution is given as follows:

$$i_{bs}(k) = -\frac{\omega_1/Q + \omega_2 p + 3600\omega_3 B}{7200\omega_3 A} \tag{17}$$

Linear programming is used to solve the function. The given value of the battery current at the $(k+1)$th sampling time $i_{bg}(k+1)$ is determined by the solution and constraints.

3.3 Dynamic power distribution

Based on the MOCO function, the power values distributed to the battery and SC are obtained. The power distribution scheme at the $(k+1)$th sampling time can be expressed as:

$$\begin{cases} P_{bg}(k+1) = U_b(k) i_{bg}(k+1) \\ P_{SCg}(k+1) = U_{SC}(k) i_{SCg}(k+1) \end{cases} \tag{18}$$

where

$$i_{SCg}(k+1) = i_{bus}(k) - i_{bg}(k+1)$$

The BESS and SC ESS are strictly controlled according to the power distribution scheme. The MOCO method makes the scheme in real time. Then the time-dependent scheme constitutes the dynamic power distribution strategy.

A flow chart of the optimization process is shown in Fig. 4. As can be seen in this figure, the MOCO solution is calculated according to the measured values at the current time and Eq. (17). After comparing the constraint values of the battery current with the MOCO solution, the given value of the battery current at the next moment is determined. The power distribution scheme is obtained according to Eq. (18).

3.4 MOCO control model in Simulink

The control model in Simulink is shown in Fig. 5. By this model, the operating states and the given currents of energy storage systems are determined. Then the charge and discharge control of energy storage systems is completed. Finally, the scheduling of the BESS and SC ESS in the HESS is effectively realized under the dynamic power distribution strategy using MOCO.

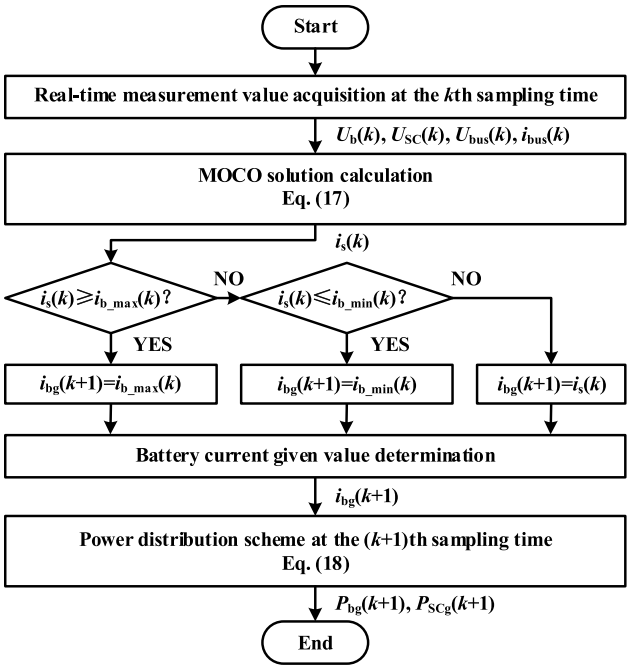

Fig. 4 Flow chart of the optimization process

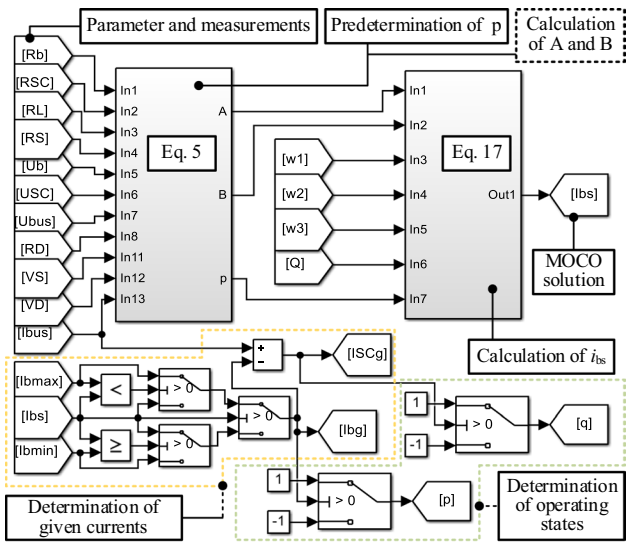

Fig. 5 Simulink control model

4 Simulation results

To validate the feasibility of the dynamic power distribution strategy using MOCO, simulations under the WLTC are carried out in MATLAB/Simulink. Simulations are performed with a BESS, a HESS using the split-frequency method, and a HESS using the proposed method, respectively.

The powers of the battery and SC are shown in Fig. 6. Table 2 lists the results of a performance comparison. The simulation results are analyzed as described below.

As shown in Fig. 7, both the battery and the SC work within the specified SOC range. The SOC drops of the battery are compared in Table 2. The ΔSOC_b in the HESS using the proposed method is 42% lower than that in the BESS, and 19% lower than that in the HESS using the split-frequency method. To sum up, the HESS with the dynamic power distribution strategy using MOCO is valid in terms of the EV range extension.

The current and current change rate of the battery are compared in Fig. 8. In the HESS using the proposed method, the SC reasonably bears the surge current when the demand power changes drastically. Thus, the battery is effectively protected. As can be seen, the magnitude, fluctuation, and change rate of the battery current in Fig. 8c are significantly smaller than those in the others.

Table 2 Simulation performance comparison

Simulation	ΔSOC_b	ΔQ_b	$\Delta Q_b'$	ΔQ_{bd}	E_{loss}
a	51.12	26.06	6.13	10.12	5.15×10^5
b	36.77	20.01	2.84	6.27	6.77×10^5
c	29.67	10.62	2.37	4.02	4.01×10^5

Where a, b and c indicate the same as Fig. 6

Table 3 lists four parameters related to the battery current during the test cycle. The four parameters are significantly reduced in the HESS using the proposed method. First, i_{max} is 71% smaller than that in the BESS, and 58% smaller than that in the HESS using the split-frequency method. Second, at the demand power peak, $|i|_{ave}$ is 60% smaller than that in the BESS, and 48% smaller than that in the HESS using the split-frequency method. Third, $|i'|_{max}$ is 77% smaller than that in the BESS, and 41% smaller than that in the HESS using the split-frequency method. Fourth, $|i'|_{ave}$ is 67% smaller than that in the BESS, and 33% smaller than that in the HESS using the split-frequency method.

As shown in Table 2, ΔQ_b is 59% smaller than that in the BESS, and 47% smaller than that in the HESS using the split-frequency method. In addition, $\Delta Q_b'$ is 61% smaller than that in the BESS, and 17% smaller than that in the HESS using the split-frequency method. Finally, ΔQ_{bd} in the HESS using the proposed method is 60% smaller than that in the BESS, and 36% smaller than that in the HESS using the split-frequency method.

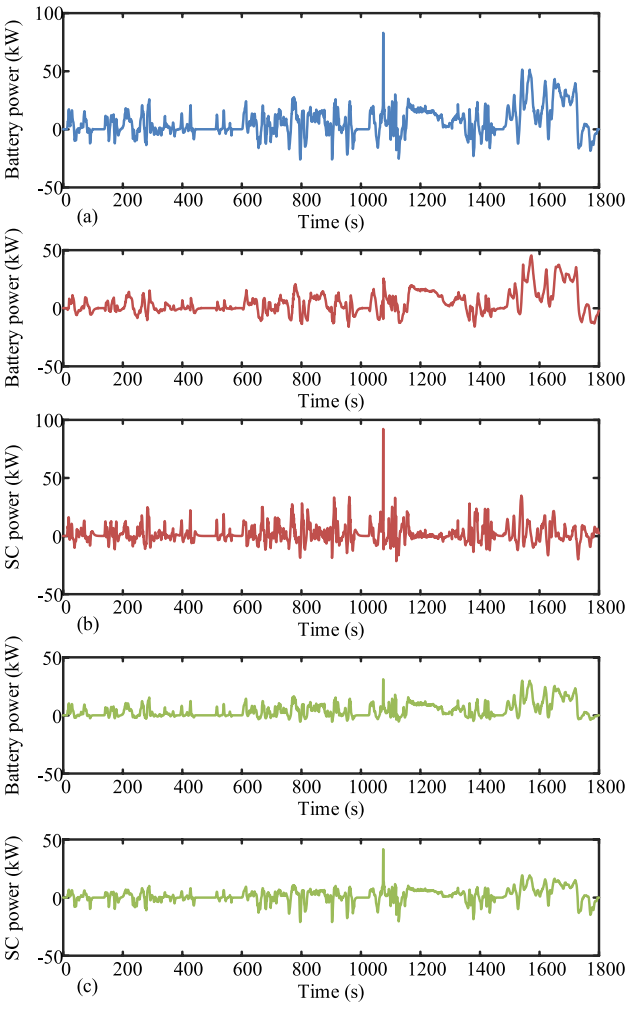

Fig. 6 Power of the battery and the SC in simulations: **a** BESS; **b** HESS using the split-frequency method; **c** HESS with the dynamic power distribution strategy using MOCO

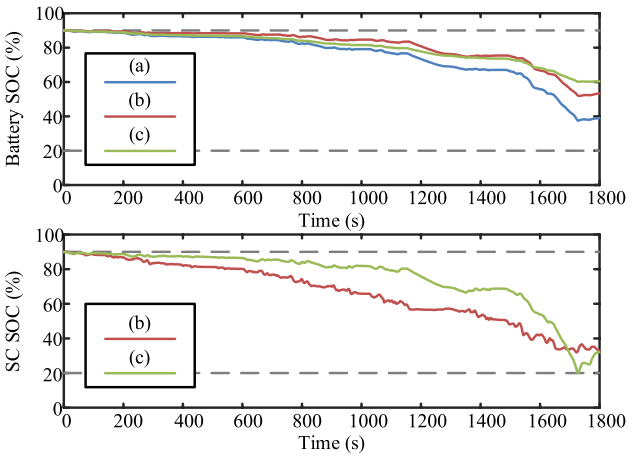

Fig. 7 Battery SOC and SC SOC in simulations: **a** BESS; **b** HESS using the split-frequency method; **c** HESS with the dynamic power distribution strategy using MOCO

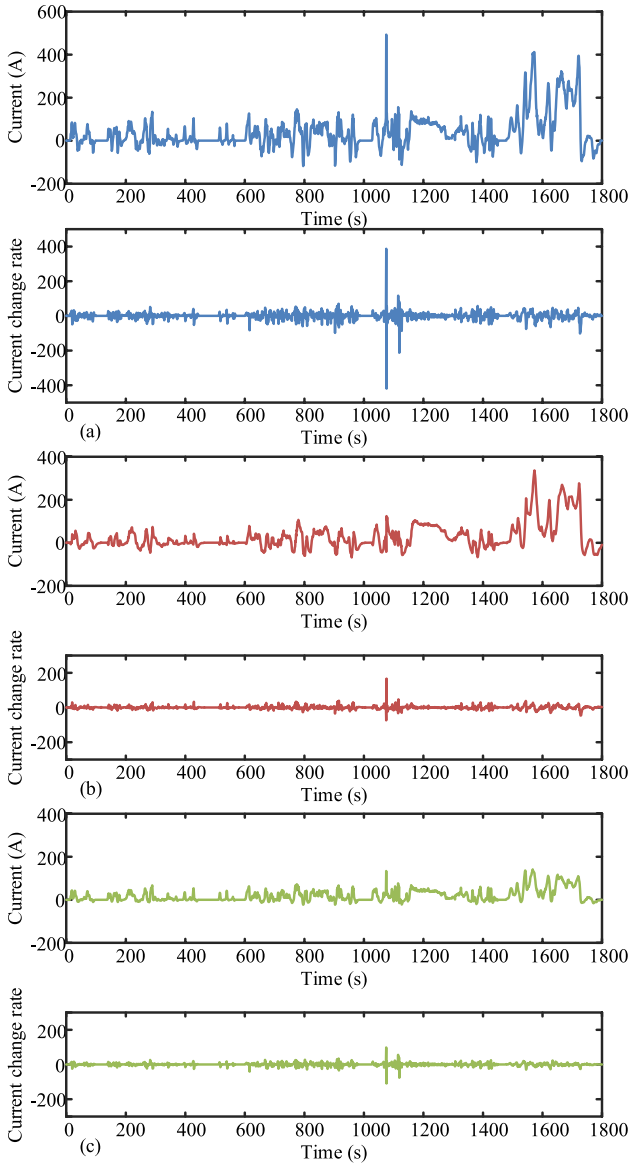

Fig. 8 Current and current change rates of the battery in simulations: **a** BESS; **b** HESS using the split-frequency method; **c** HESS with the dynamic power distribution strategy using MOCO

Table 3 Simulation parameters

Simulation	i_{max}	$\|i\|_{ave}$	$\|i'\|_{max}$	$\|i'\|_{ave}$
a	493	52	419	12
b	337	40	166	6
c	141	21	98	4

Where a, b and c indicate the same as Table 2; i_{max} indicates the maximum battery current; $|i|_{ave}$ indicates the average value of the absolute value of the battery current; $|i'|_{max}$ indicates the maximum absolute value of the battery current change rate; and $|i'|_{ave}$ indicates the average value of the absolute value of the battery current change rate

These results illustrate that the HESS with the dynamic power distribution strategy using MOCO can significantly mitigate battery degradation.

The energy loss is also listed in Table 2. E_{loss} using the proposed method is 22% less than that in the BESS, and 41% less than that in the HESS using the split-frequency method. Therefore, it can be considered that the dynamic power distribution strategy using MOCO can appropriately reduce the HESS energy loss.

Taken together, it can be considered that the HESS with the dynamic power distribution strategy using MOCO exhibits its obvious superiority. After the above analyses, the feasibility of the dynamic power distribution strategy is verified.

5 Experimental results

To further validate the effectiveness of the dynamic power distribution strategy using MOCO, experiments under the WLTC are carried out on a constructed motor experimental platform. The HESS is scaled down to fit the motor. The permanent magnet synchronous motor experimental platform is shown in Fig. 9. Two coaxial motors are used. However, one of them is not connected to the system. By controlling the speed difference between the two motors, the motor in the system is in the driving or braking state, thereby simulating an EV.

According to the speed relationship between the vehicle and the motor, the given motor rotation speed can be calculated. At the given rotation speed, the DC bus power is measured in the experiment. The motor rotation speed and measured demand power are shown in Fig. 10. The driving energy in the DC bus is 319 kJ, and the braking energy in the DC bus is 78 kJ.

The power of the battery and SC is shown in Fig. 11. Table 4 gives the results of a performance comparison. The experimental results are analyzed as described below.

The battery SOC and SC SOC are shown in Fig. 12. The SOC drops of the battery are compared in Table 4. The

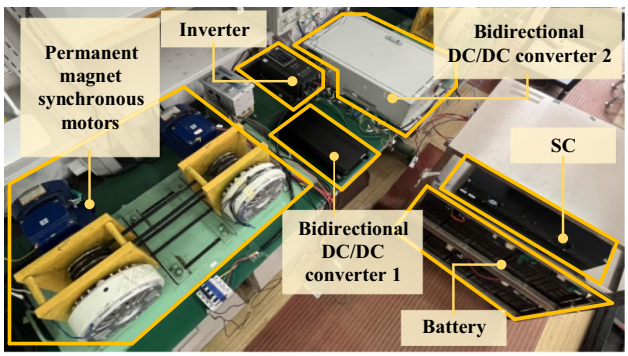

Fig. 9 Permanent magnet synchronous motors experimental platform

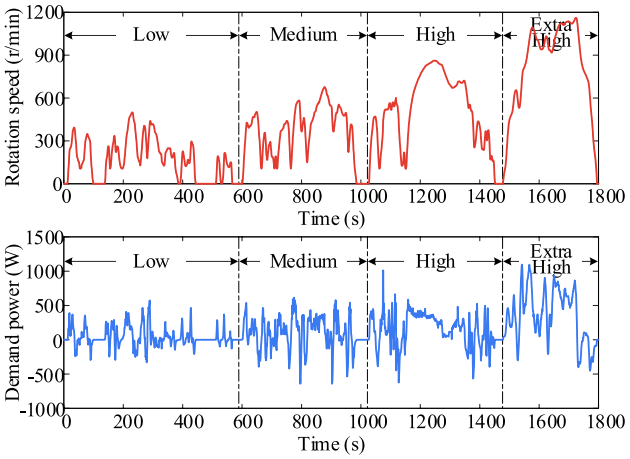

Fig. 10 Given motor speed and measured demand power

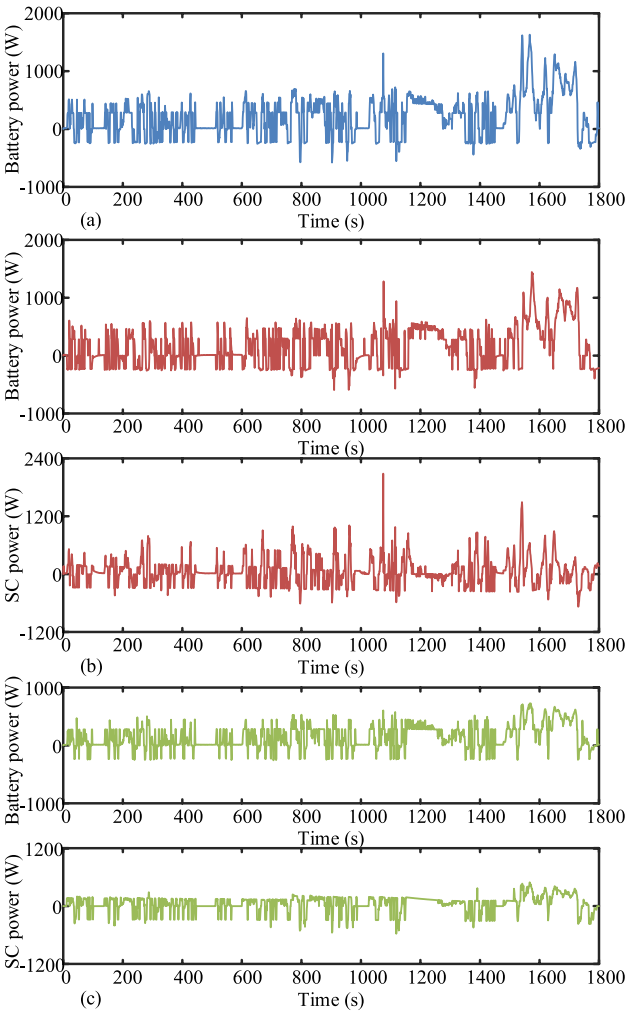

Fig. 11 Power of the battery and the SC in experiments: **a** BESS; **b** HESS using the split-frequency method; **c** HESS with the dynamic power distribution strategy using MOCO

Table 4 Experimental performance comparison

Experiment	ΔSOC_b	ΔQ_b	$\Delta Q_b'$	ΔQ_{bd}	E_{loss}
a	1.33	0.73	0.21	0.31	5.45×10^4
b	1.10	0.68	0.24	0.33	5.89×10^4
c	0.92	0.44	0.17	0.22	2.71×10^4

Where a, b and c indicate the same as Fig. 11

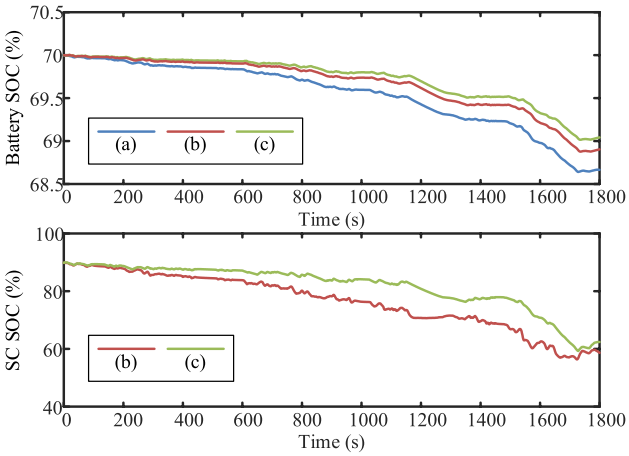

Fig. 12 Battery SOC and SC SOC in experiments: **a** BESS; **b** HESS using the split-frequency method; **c** HESS with the dynamic power distribution strategy using MOCO

ΔSOC_b in the HESS using the proposed method is 31% lower than that in the BESS, and 16% and lower than that in the HESS using the split-frequency method. In short, the HESS with the dynamic power distribution strategy using MOCO is valid in terms of EV range extension.

The current and current change rate of the battery are compared in Fig. 13. As can be seen, the magnitude, fluctuation and change rate of the battery current in the HESS using the proposed method are significantly smaller than those in other methods. The battery is protected since the SC withstands current peaks and smoothens power fluctuations.

Table 5 lists four parameters related to the battery current during the test cycle. Their definitions are the same as those in the simulation. First, i_{max} is 56% smaller than that in the BESS, and 50% smaller than that in the HESS using the split-frequency method. Second, at the demand power peak, $|i|_{ave}$ is 40% smaller than that in the BESS, and 36% smaller than that in the HESS using the split-frequency method. Third, $|i'|_{max}$ is 42% smaller than that in the BESS, and 55% smaller than that in the HESS using the split-frequency method. Fourth, $|i'|_{ave}$ is 25% smaller than that in the BESS, and 40% smaller than that in the HESS using the split-frequency method.

As shown in Table 4, ΔQ_b is 40% smaller than that in the BESS, and 35% smaller than that in the HESS using

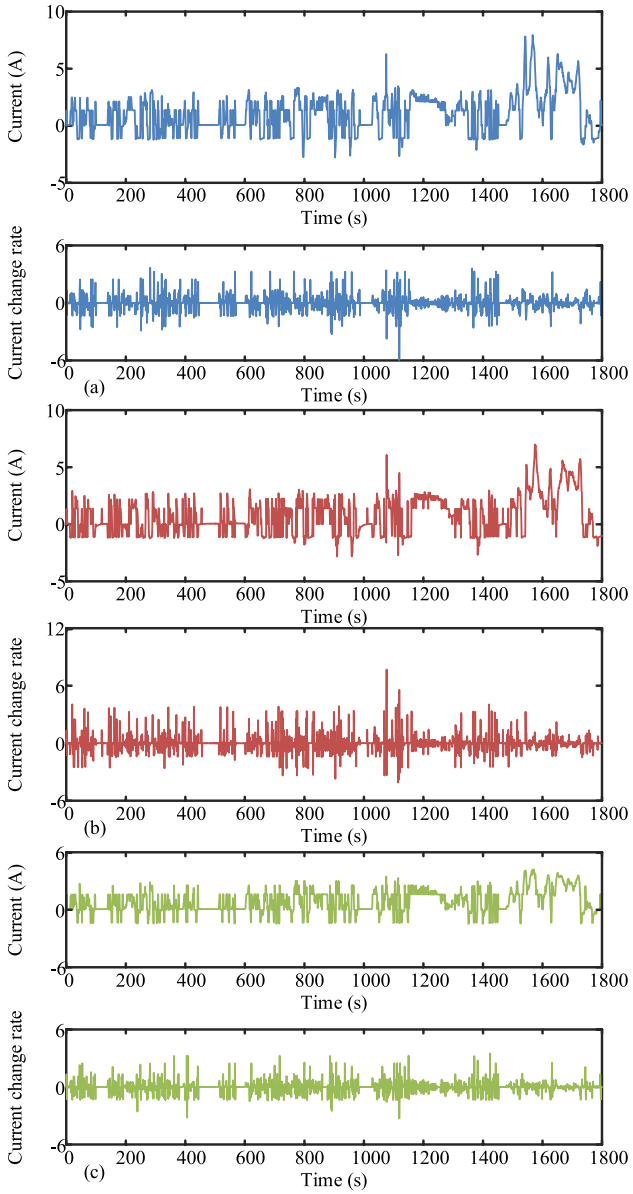

Fig. 13 Current and current change rates of the battery in experiments: **a** BESS; **b** HESS using the split-frequency method; **c** HESS with the dynamic power distribution strategy using MOCO

Table 5 Experimental parameters

Experiments	i_{max}	$\|i\|_{ave}$	$\|i'\|_{max}$	$\|i'\|_{ave}$
a	8.0	1.5	6.0	0.4
b	7.0	1.4	7.7	0.5
c	3.5	0.9	3.5	0.3

Where a, b and c indicate the same as Table 4

the split-frequency method. In addition, $\Delta Q_b'$ is 19% smaller than that in the BESS, and 29% smaller than that in the HESS using the split-frequency method. Finally, ΔQ_{bd} in the HESS using the proposed method is 29% smaller than that in the BESS, and 33% smaller than that in the HESS using the split-frequency method.

These results illustrate that the HESS with the dynamic power distribution strategy using MOCO has excellent performance in terms of battery degradation mitigation.

The energy loss is also listed in Table 4. E_{loss} using the proposed method is 50% less than that in the BESS, and 54% less than that using the split-frequency method. Therefore, it can be seen that the dynamic power distribution strategy using MOCO can reduce the HESS energy loss.

It can be seen that the HESS with the dynamic power distribution strategy using MOCO has a significant advantage. After the above analyses, the effectiveness of the dynamic power distribution strategy is verified.

6 Conclusion

This paper proposed a dynamic power distribution strategy using MOCO for an EV with a HESS. EV range extension, battery degradation mitigation, and HESS energy loss reduction were taken into account in MOCO. Taking the battery current as the control variable, the MOCO function was established and solved to obtain the current solution. The power distribution scheme was derived from this solution. On this basis, real-time dynamic power distribution was constructed by constantly solving the function and updating the scheme. In the HESS, the scheduling of the BESS and the SC ESS was completed.

Through the simulations and experiments under the WLTC, the following conclusions were drawn. The HESS using the proposed method can effectively alleviate the contradictions among three objectives. It made great progress in EV range extension, battery degradation mitigation, and HESS energy loss reduction. By using the proposed method, the EV range extension was improved by an average of 31% in the simulation and 24% in the experiment, respectively. The battery degradation mitigation was improved by an average of 48% in the simulation and 31% in the experiment, respectively. The HESS energy loss reduction was improved by an average of 32% in the simulation and 52% in the experiment, respectively.

Acknowledgements The authors thank the National Natural Science Foundation of China (No. 51775363) and the Key Research and Development Projects of Shanxi Province (No. 201803D121124) for funding this research project.

Data availability Data will be made available on request.

Declarations

Conflict of interest On behalf of all authors, the corresponding author states that there is no conflict of interest.

References

1. Wang, Y., Wang, L., Li, M., Chen, Z.: A review of key issues for control and management in battery and ultra-capacitor hybrid energy storage systems. eTransportation **4**, 1 (2020)
2. Babu, T., Vasudevan, K., Ramachandaramurthy, V., Sani, S., Chemud, S., Lajim, R.: A comprehensive review of hybrid energy storage systems: converter topologies, control strategies and future prospects. IEEE Access **8**, 148702–148721 (2020)
3. Song, Z., Hofmann, H., Li, J., Han, X., Zhang, X., Ouyang, M.: A comparison study of different semi-active hybrid energy storage system topologies for electric vehicles. J. Power Sources **274**, 400–411 (2015)
4. Lu, X., Wang, H.: Optimal sizing and energy management for cost-effective PEV hybrid energy storage systems. IEEE Trans. Ind. Informat. **16**(5), 3407–3416 (2020)
5. Liu, Y., Li, Z., Lin, Z., Zhao, K., Zhu, Y.: Multi-objective optimization of energy management strategy on hybrid energy storage system based on Radau Pseudospectral method. IEEE Access **7**, 112483–112493 (2019)
6. Liao, H., Peng, J., Wu, Y., Li, H., Zhou, Y., Zhang, X., Huang, Z.: Adaptive split-frequency quantitative power allocation for hybrid energy storage systems. IEEE Trans. Transport. Electrific. **7**(4), 2306–2317 (2021)
7. Hredzak, B., Agelidis, V., Demetriades, G.: A low complexity control system for a hybrid DC power source based on ultracapacitor-lead-acid battery configuration. IEEE Trans. Power Electron. **29**(6), 2882–2891 (2014)
8. Peng, J., Wang, R., Liao, H., Zhou, Y., Li, H., Wu, Y., Huang, Z.: A real-time layer-adaptive wavelet transform energy distribution strategy in a hybrid energy storage system of EVs. Energies **12**(3), 1 (2019)
9. Wang, B., Xu, J., Cao, B., Zhou, X.: A novel multimode hybrid energy storage system and its energy management strategy for electric vehicles. J. Power Sources **281**, 432–443 (2015)
10. Li, Y., Huang, X., Liu, D., Wang, M., Xu, J.: Hybrid energy storage system and energy distribution strategy for four-wheel independent-drive electric vehicles. J. Clean. Prod. **220**, 756–770 (2019)
11. Zhang, H., Zhang, F., Yang, L., Gao, Y., Jin, B.: Multi-parameter collaborative power prediction to improve the efficiency of supercapacitor-based regenerative braking system. IEEE Trans. Energy Convers. **36**(4), 2612–2622 (2021)
12. Naseri, F., Farjah, E., Ghanbari, T.: An efficient regenerative braking system based on battery/supercapacitor for electric, hybrid and plug-in hybrid electric vehicles with BLDC motor. IEEE Trans. Veh. Technol. **66**(5), 3724–3738 (2017)
13. Bindu, R., Thale, S.: Power management strategy for an electric vehicle driven by hybrid energy storage system. IETE J. RES. **68**(4), 2801–2811 (2022)
14. Mali, V., Tripathi, B.: Thermal stability of supercapacitor for hybrid energy storage system in lightweight electric vehicles: Simulation and experiments. J. Mod. Power Syst. Cle. **10**(1), 170–178 (2022)
15. Gomozov, O., Trovao, J., Kestelyn, X., Dubois, M.: Adaptive energy management system based on a real-time model predictive control with nonuniform sampling time for multiple energy storage electric vehicle. IEEE Trans. Veh. Technol. **66**(7), 5520–5530 (2017)
16. Li, M., Wang, L., Wang, Y., Chen, Z.: Sizing optimization and energy management strategy for hybrid energy storage system using multi-objective optimization and random forests. IEEE Trans. Power Electron. **36**(10), 11421–11430 (2021)
17. Song, Z., Hofmann, H., Li, J., Hou, J., Han, X., Ouyang, M.: Energy management strategies comparison for electric vehicles with hybrid energy storage system. Appl. Energy **134**, 321–331 (2014)
18. Liu, C., Wang, Y., Chen, Z.: Degradation model and cycle life prediction for lithium-ion battery used in hybrid energy storage system. Energy **166**, 796–806 (2019)
19. Nguyen, B., German, R., Trovao, J., Bouscayrol, A.: Real-time energy management of battery/supercapacitor electric vehicles based on an adaptation of Pontryagin's minimum principle. IEEE Trans. Veh. Technol. **66**(1), 203–212 (2019)
20. Wang, L., Wang, Y., Liu, C., Yang, D., Chen, Z.: A power distribution strategy for hybrid energy storage system using adaptive model predictive control. IEEE Trans. Power Electron. **35**(6), 5897–5906 (2020)
21. Liu, C., Wang, Y., Wang, L., Chen, Z.: Load-adaptive real-time energy management strategy for battery/ultracapacitor hybrid energy storage system using dynamic programming optimization. J. Power Sources **438**, 1 (2019)
22. Cheng, L., Wang, W., Wei, S., Lin, H., Jia, Z.: An improved energy management strategy for hybrid energy storage system in light rail vehicles. Energies **11**(2), 1 (2018)
23. Li, C., Liu, G.: Optimal fuzzy power control and management of fuel cell/battery hybrid vehicles. J. Power Sources **192**(2), 525–533 (2019)
24. Wang, Y., Yang, Z., Lin, F., An, X., Zhou, H., Fang, X.: A hybrid energy management strategy based on line prediction and condition analysis for the hybrid energy storage system of tram. IEEE Trans. Ind Appl. **56**(2), 1793–1803 (2020)
25. Shen, J., Khaligh, A.: A supervisory energy management control strategy in a battery/ultracapacitor hybrid energy storage system. IEEE Trans. Transport. Electrific. **1**(3), 223–231 (2015)
26. Anbazhagan, G., Jayakumar, S., Muthusamy, S., Sundararajan, S., Panchal, H., Sadasivuni, K.: An effective energy management strategy in hybrid electric vehicles using Taguchi based approach for improved performance. Energ. Source Part A **44**, 3418–3435 (2022)
27. Hou, J., Song, Z.: A hierarchical energy management strategy for hybrid energy storage via vehicle-to-cloud connectivity. Appl. Energy **257**, 1 (2020)

Yuqing Shao was born in Shandong, China, in 1997. She received her B.S. degree in Electrical Engineering from the Taiyuan University of Technology, Taiyuan, China, in 2020, where she is presently working towards her M.S. degree. Her current research interests include hybrid energy storage technology and energy management strategies.

Hongjuan Zhang was born in Shanxi, China, in 1974. She received her B.S. and M.S. degrees in Power Electronics and Automation, and her Ph.D. degree in Mechatronic Engineering from the Taiyuan University of Technology, Taiyuan, China, in 2011. She is presently working as a professor in the College of Electrical and Power Engineering, Taiyuan University of Technology. She is the author of more than 30 articles and the creator of more than 20 national inventions. Her current research interests include electrical energy-saving technology, electrical testing technology, and new power electronics technology.

Yan Gao was born in Shanxi, China, in 1969. She received her M.S. degree in Automation from the Taiyuan University of Technology, Taiyuan, China, in 1998. She is presently working as an Associate Professor in College of Electrical and Power Engineering, Taiyuan University of Technology, Taiyuan, China. She is the author of more than 20 articles and the creator of more than 20 national inventions. Her current research interests include electrical detection technology and automatic control technology.

Baoquan Jin was born in Shanxi, China, in 1972. He received his M.S. and Ph.D. degrees in Mechatronic Engineering from the Taiyuan University of Technology, Taiyuan, China, in 2003 and 2010, respectively. He is presently working as a professor and as deputy director of the Key Laboratory of Advanced Transducers and Intelligent Control Systems of the Ministry of Education and Shanxi Province, Taiyuan University of Technology. He is the author of more than 50 articles and the creator of more than 40 national inventions. His current research interests include intelligent control, intelligent sensing, and detection technology.